ACS APPLIED MATERIALS & INTERFACES

Research Article

www.acsami.org

Embedded into Graphene Ge Nanoparticles Highly Dispersed on Vertically Aligned Graphene with Excellent Electrochemical Performance for Lithium Storage

Shuaixing Jin, Na Li, Hao Cui, and Chengxin Wang*

State Key Laboratory of Optoelectronic Materials and Technologies, School of Physics Science and Engineering, Sun Yat-sen (Zhongshan) University, Guangzhou 510275, P. R. China

Supporting Information

ABSTRACT: Decreasing particle size has always been reported to be an efficient way to improve cyclability of Li-alloying based LIBs. However, nanoparticles (NPs) tend to agglomerate and evolve into lumps, which in turn limits the cycling performance. In this report, we prepared a unique nanostructure, graphene-coated Ge NPs are highly dispersed on vertically aligned graphene (Ge@graphene/VAGN), to avoid particle agglomeration and pulverization. Remarkable structure stability of the sample leads to excellent cycling stability. Upon cycling, the anode exhibits a high capacity of 1014 mAh g^{-1}, with nearly no capacity loss in 90 cycles. Rate performance shows that even at the high current density of 13 A g^{-1}, the anode could still deliver a higher capacity than that of graphite.

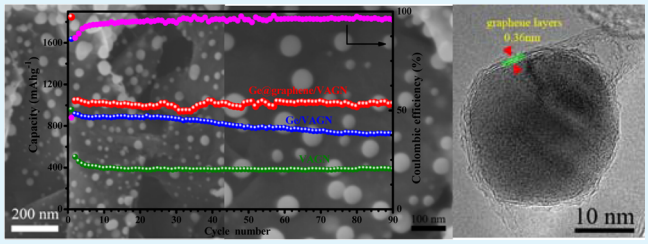

KEYWORDS: *lithium-ion batteries, Ge NPs, graphene coating, binder free, vertically aligned graphene, cyclability*

INTRODUCTION

In recent years, germanium (Ge) has attracted much research interest due to its potential application in next generation lithium ion batteries (LIBs).[1−3] As a typical Li-alloying anode material, Ge could store 4.4 Li atoms during the Li-alloying process and deliver a theoretical capacity up to 1623 $mAhg^{-1}$, which is 4 times higher than that of the commercial graphite anode (only 372 $mAhg^{-1}$).[4] Moreover, Ge possesses a relatively low working potential vs Li/Li^+ (∼300 mv); thus, it can be favorably combined with those high voltage cathode materials.[5,6] Therefore, Ge is a promising alternative to graphite to assemble higher-energy and higher-power density LIBs. Nevertheless, the poor cycling stability has always been the bottleneck for the practical application of Ge. Upon the lithiated/delithiated process, Ge suffers drastic volume changes (370%), which will induce pulverization of the bulk material and finally leads to isolation between the particle and the current collector.[7−9] Consequently, rapid capacity loss inevitably occurs.

Decreasing particle size of the bulk Ge electrode has been found to be an effective approach to alleviate the volume changes. Various nanosized Ge anodes were reported in previous studies, such as nanoparticles,[10−12] nanowires,[13,14] nanotubes,[15] and so forth. Nanosized materials, for instance, nanoparticles, possess a larger surface area and can provide more active reaction point for Li^+. More importantly, nanoparticles suffer smaller absolute volume changes than their bulk counterparts do, which could minimize cracking and pulverization of the anode. However, the naked, densely distributed nanoparticles tend to aggregate and evolve into lumps, which not only limits the lithium ion diffusion pathway but also means the electrode pulverization could reappear.[16,17] In some recent studies, carbon-coated nanoparticles have been prepared to prevent direct contacts of the particle.[17−21] Nevertheless, the densely agglomerate nature of NPs still existed, leading to unsatisfactory cycling performance.

In this report, we prepared highly dispersed Ge NPs under the aid of in situ grown graphene to tackle the above problem. As Scheme 1 shows, Ge nanoparticles are wrapped by 2−3 graphene layers and uniformly distributed on both sides of vertically aligned graphene (VAGN). This hybrid nanostructure has two superiorities in applying to LIBs. On the one hand, particle aggregations are eliminated since Ge NPs isolate from each other. Meanwhile, VAGN sheets are directly grown on substrate and possess large interspaces between each other, which can avoid the common drawback of stacking for conventional graphene.[22,23] On the other hand, particle pulverizations are also alleviated. Graphene layers coated on Ge NPs can effectively buffer the volume changes and accommodate the accompanying mechanical stress. With these structure advantages, improved cycling stability could be expected. The sample was directly assembled into LIBs without any binders or conductive materials and exhibited excellent cycling performances. A stable capacity of 1014 mAh

Received: August 15, 2014
Accepted: October 24, 2014
Published: October 24, 2014

   dx.doi.org/10.1021/am505499x | ACS Appl. Mater. Interfaces 2014, 6, 19397−19404

Scheme 1. Schematic Illustration for the Ge@graphene/VAGN Hybrid Nanostructures and the Electrode Changes upon Discharge/Charge Process

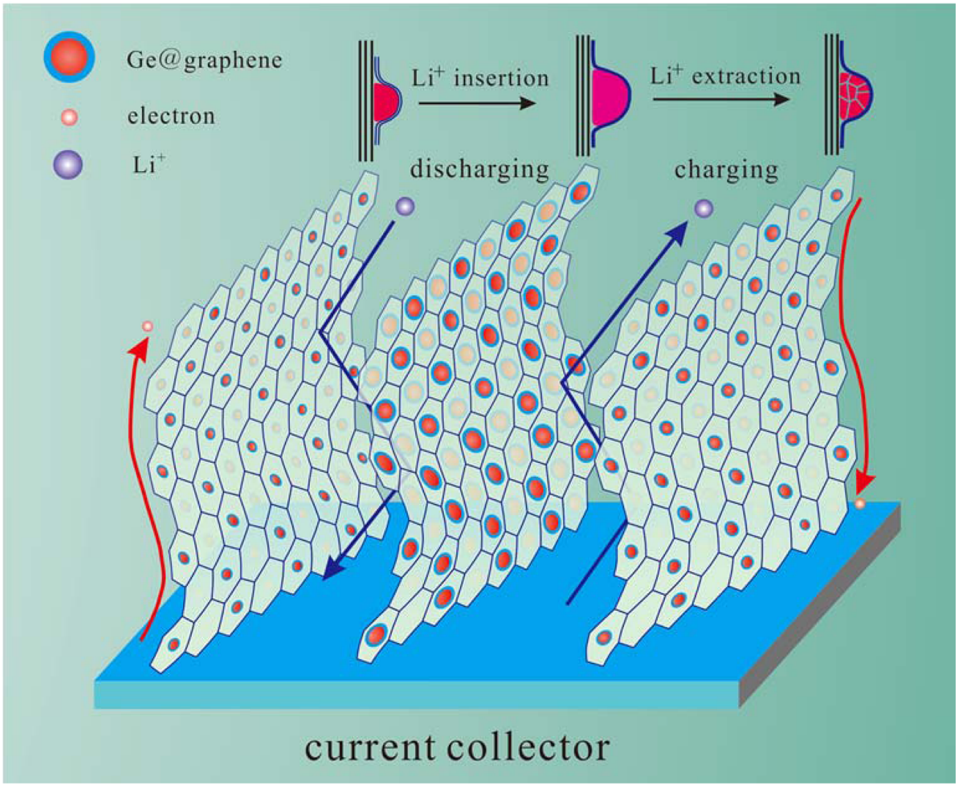

g^{-1} was recorded after 90 cycles, with a capacity retention more than 97%. Rate performance shows at the high current density of 13 A g^{-1}, a high capacity of 420 mAh g^{-1} still maintained. These results demonstrate that the surface protected, highly dispersed NPs could effectively improve the cyclability of Ge-based LIBs, which also provides a solution for other similar Li-alloying anode such as Si and Sn.

EXPERIMENTAL SECTION

The final products, Ge@graphene/VAGN, were reduced from GeO_2/VAGN by H_2/CH_4 hybrid plasma. The detailed synthesis procedures are depicted as follows.

VAGN was synthesized in a 2 KW, 2.5 GHz microwave plasma enhanced chemical vapor deposition (MPECVD) system. A round copper foil (d = 7 mm, 0.38 mm^2) cleaned by ethanol and deionized water in sequence was used as substrate. Placed into center of the MPECVD chamber, the substrate was first heated to 380 °C by H_2 plasma at a power of 600 W. The pressure and flow rate of hydrogen was 6 Torr, 30 sccm, respectively. When the system reached the desired temperature, H_2 flow was changed to 20 sccm and a CH_4 flow of 10 sccm was introduced simultaneously. After 2 min deposition, the plasma was terminated and VAGN was obtained.

GeO_2 films were deposited to VAGN by a thermal GeO_2/Sn coevaporation method in a conventional horizontal tube furnace, which is modified from previous studies.[13,24] High purity GeO_2 powders (10 mg) (Aladdin, 99.999%) and 40 mg tin powders (Aladdin, 99.99%) were thoroughly mixed and located at the thermal center. A piece of VAGN was placed at the low-temperature region to receive the sediments. The furnace was slowly heated to 700 °C at a rate of 5 °C/min and then kept for 15 min before cooling. During the whole process, the chamber pressure was maintained lower than 1 Torr.

In the next step, GeO_2 films were reduced to Ge nanoparticles and coated by graphene layers at the same time. The as-synthesized GeO_2/VAGN was placed in the center of the MPECVD chamber, and the system was evaporated to 0.5 Torr. After that, the chamber pressure was raised to 5 Torr by a H_2 flow of 30 sccm. Then, the plasma source was turned on at a power of 500 W and kept for 20 s. Next, H_2 flow was decreased to 20 sccm and a CH_4 flow of 10 sccm was introduced. This hybrid plasma condition was kept for 5 s before cooling down to the room temperature.

Three kinds of Ge-load samples were synthesized. And it is a coeffect of the synthesis steps to obtain the different sample. Namely, the reaction time for GeO_2 deposition and reduction are all set according to the target product. Detailed reaction time could be seen in Supporting Information Table S1. The control sample, bare Ge NPs anchored on VAGN (Ge/VAGN), was obtained under the similar conditions to the 55 wt % sample (same GeO_2 deposition time and H_2 plasma reduction time), with no introduction of CH_4 plasma after the reduction procedure.

CHARACTERIZATION

A Quanta 400F field emission scanning electronic microscopy (FESEM, 20 kV) and a FEI Tecnai G2 F30 transmission electron microscopy (TEM, 300 kV) were used to observe the morphologies of the as-prepared samples. Crystal structure and chemical composition were characterized by X-ray diffraction (XRD, D/MAX 2200 VPC) with Cu Kα radiation, Raman spectroscopy, and energy dispersive spectroscopy (EDS). Mass of the active materials was accurately weighed by a micro-balance with readability of 0.1 μg (METTLER-TOLED AG, XP2U, Switzerland). Results of the mass measurement could be seen in Supporting Information Table S2.

ELECTROCHEMICAL MEASUREMENTS

The as-prepared Ge@graphene/VAGN hybrids were directly assembled into LIBs for electrochemical tests. A lithium foil was used as counter electrode and the separator was polypropylene

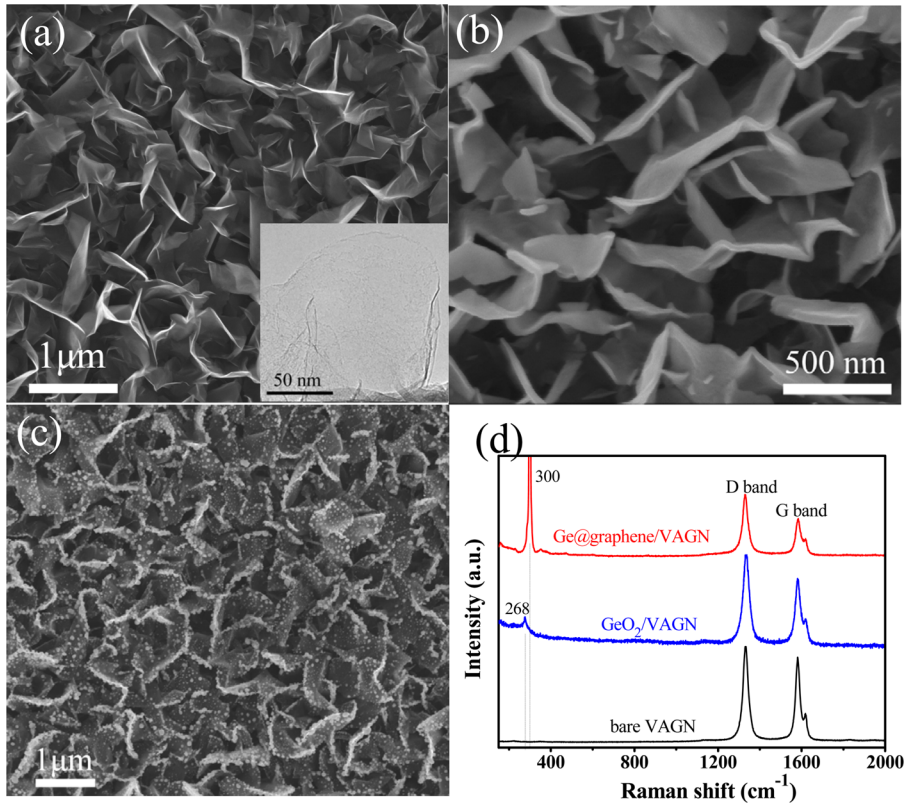

Figure 1. Morphologies of the products from each synthesis step. (a) Vertically aligned graphene (VAGN), the inset is TEM image of a single graphene sheet; (b) GeO_2/VAGN, graphene sheets are uniformly wrapped by GeO_2 sediments on both sides; (c) Ge@graphene/VAGN, GeO_2 was reduced to Ge by H_2/CH_4 hybrid plasma; (d) Raman spectra of the three samples.

membrane. The electrolyte was a solution of 1 M $LiPF_6$ in mixed solvent of ethylene carbonate (EC) and diethyl carbonate (DEC) with a mass ratio of 1:1. Cyclic voltammetry was tested on an Ivium electrochemical workstation wtihin the voltage window of 0−3 V. Galvanostatic charge/discharge tests were carried out on a BT-2000 battery tester (Arbin Instruments, College station, TX) in the voltage range 0.01∼1.5 V.

RESULTS AND DISCUSSION

Figure 1a−c displays morphologies of the product from each synthesis step and the corresponding Raman spectra are shown in Figure 1d. Figure 1a is the bare VAGN. It can be seen the flexible graphene sheets arbitrarily interlace with each other. Cross-section SEM image (Supporting Information Figure S1) shows the nanosheets have a vertical alignment with respect to the Cu substrate. The VAGN nanosheets possess ultrathin thickness and smooth surface. Inset is the TEM image of a single graphene sheet, which is nearly transparent for electron beam. Raman spectrum of the bare VAGN (black line) reveals two sharp peaks at 1330 and 1578 cm^{-1}, corresponding to the disorder induced D-band and graphitic G-band, respectively.[25−27] The intensity ratio of D-band to G-band (I_D/I_G) is larger than 1, indicating the defective, low crystallinity nature of the VAGN.

After deposition, the sample evolved into thicker nanosheets, however, the vertical morphology was still maintained (Figure 1b). It could be noted that both sides of the graphene were uniformly covered by sediments. EDS shows the sample contains Cu, C, Ge, O (Figure S2). In the Raman spectrum (blue line), besides the D- and G- band, an additional peak at 268 cm^{-1} appears, which is related to the α-quartz-like GeO_2.[28,29]

During the following reduction process, GeO_2 layers were quickly changed into molten state and reduced to Ge droplets by H_2 plasma. Then the neighboring droplets joined with each other and evolved into Ge NPs. The subsequently introduced CH_4 plasma induced the nucleation and growth of graphene on the surface of Ge NPs. As Figure 1c shows, the surface of graphene sheets reappears with nanoparticles uniformly decorated on it. Synchronously, the sharp Raman peak corresponding to Ge could be observed at 300 cm^{-1} (red line).[30]

Crystal structure of the final product was further confirmed by X-ray diffraction (XRD). As Figure 2b shows, the broad peak at 26° is ascribed to (002) plane of graphene. The peaks of Ge NPs are located at 27° and 45°, which is consistent with the cubic Ge phase (JCPDS card no.04-0545).

Three samples with different Ge mass content (45%, 55%, and 70 wt %) were prepared. Figure 2a shows a clear view of the 55 wt % sample and the others are shown in Supporting Information Figure S3. It could be seen graphene sheets are homogeneously anchored by nanoparticles, and no graphene stacking or particle aggregation are observed. Based on the in situ grown VAGN, the hybrid nanosheets tightly contact with the current collector and align in unified orientation, which could provide a fast electron transport channel and a smooth Li^+ pathway upon cycling.[31] High magnification SEM images (Figure 2c and d) demonstrate that Ge NPs possess highly dispersed nature and uniform size distribution. To accurately determine the size distribution, ∼40 particles were measured (Supporting Information Figure S4) and the results were listed

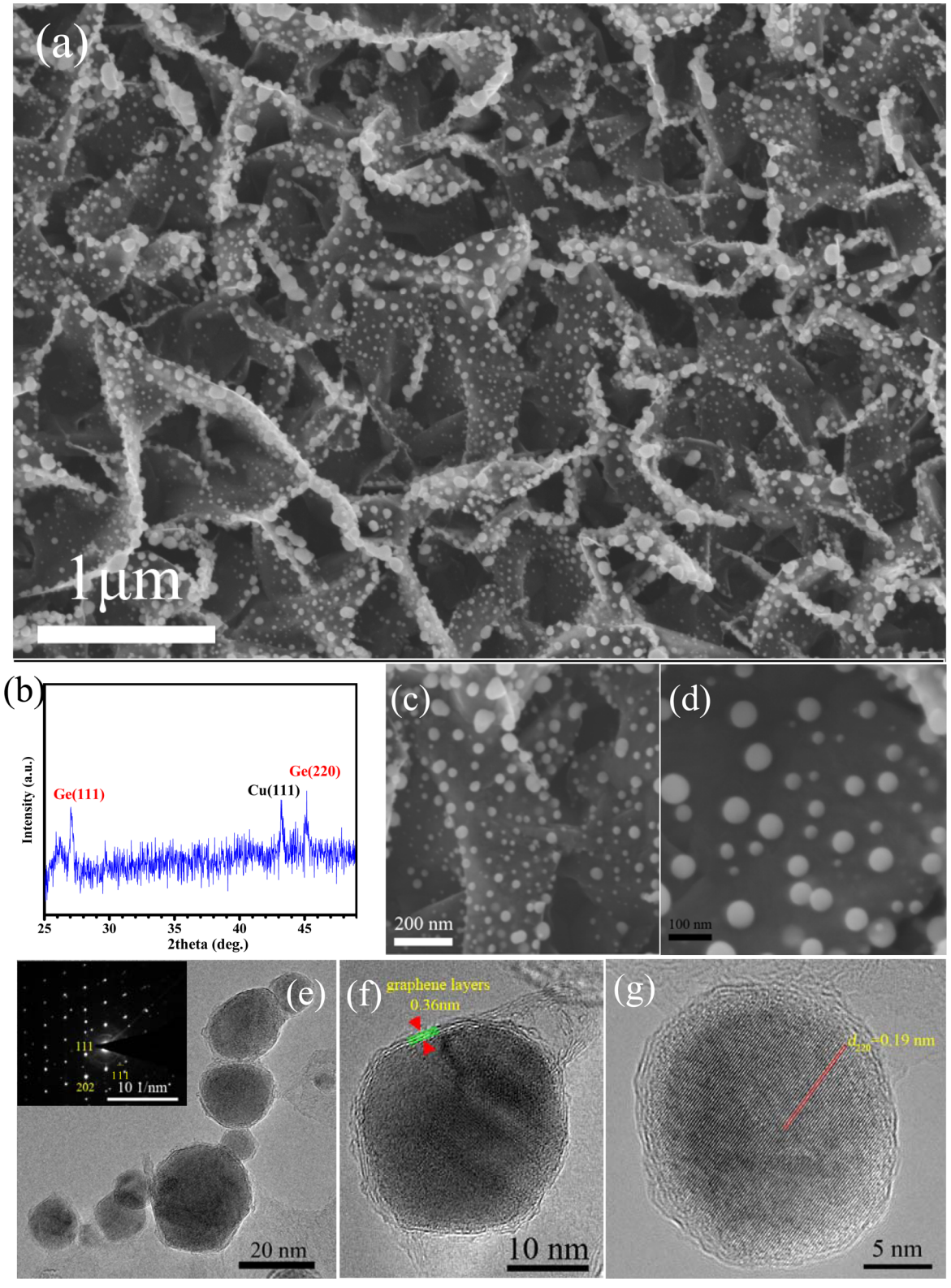

Figure 2. (a) Panoramic view of the as-prepared Ge@graphene/VAGN; (b) XRD pattern of the sample; (c and d) high magnification SEM images of the sample, showing monodispersion nature of Ge NPs; (e) TEM image of several Ge NPs, the graphene coatings could be clearly identified, inset is the SAED pattern; (f) HRTEM image of a single Ge NPs, the graphene layers are calculated to 3; (g) lattice resolved HRTEM image of Ge NPs.

in Supporting Information Table S3. According to the statistical results, average diameter of the NPs is 42 nm.

Figure 2e shows low magnification TEM image of several Ge NPs and the minimum particle in the picture is 10 nm. The selected area electron diffraction (SAED) pattern (inset image) indicates Ge NPs are in single crystalline structure and the calculating result is consistent with the XRD pattern. The single crystalline nature of Ge nanoparticle was also evidenced by high-resolution TEM image (HRTEM, Figure 2g). A lattice spacing of 0.19 nm was measured, corresponding to the (220)

dx.doi.org/10.1021/am505499x | ACS Appl. Mater. Interfaces 2014, 6, 19397−19404

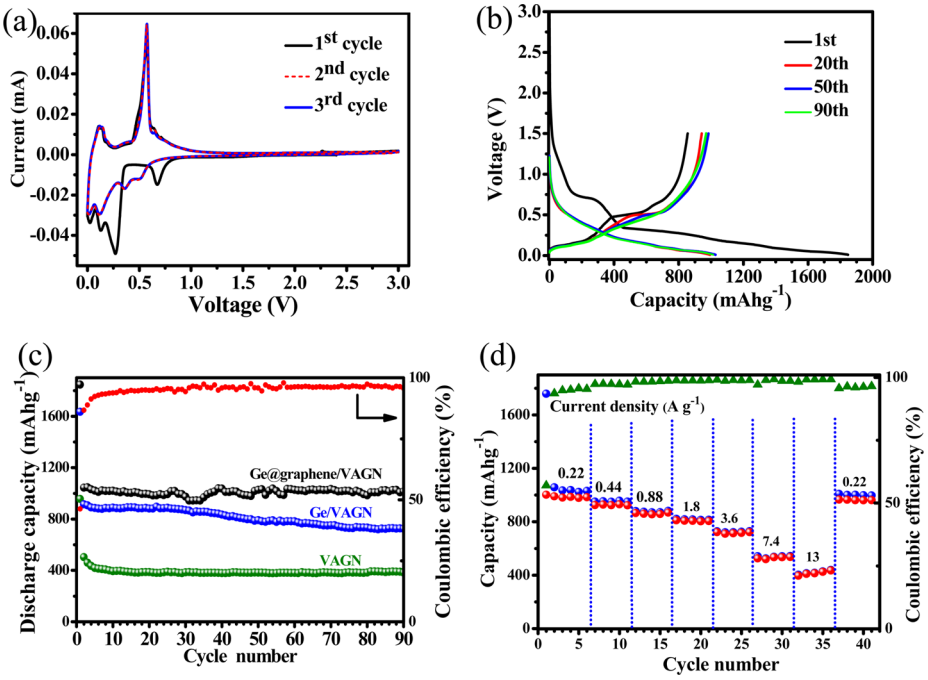

Figure 3. Electrochemical tests of the Ge@graphene/VAGN anode. (a) Cyclic voltammetry (CV) curves of the first three cycles; (b) Voltage profiles of the 55 wt % Ge content sample at a current density of 260 mA g^{-1}; (c) Cycling performace of the Ge@graphene/VAGN, Ge/VAGN and bare VAGN anode, all the cell are tested under same current density; (d) Rate performance.

plane of cubic Ge. It should be noted that in Figure 2e, graphene layers wrapping on the outermost surface of Ge NPs are easily identified. In the HRTEM image (Figure 2f), three dark lines could be seen on the periphery of the particle, indicating the graphene layer numbers are 3. The spacing distance between neighboring dark lines was measured to be 0.36 nm. The graphene coating is a favorable factor for accommodating mechanical strain and facilitating electron transfer, but the layer numbers should be moderate, since excessive gaphene layers will block the diffusion of lithium ions. According to recent study, the critical thickness for Li ions to diffuse is 6 layers.[32]

Figure 3a shows the first three cyclic voltammetry (CV) curves of the Ge@graphene/VAGN electrode in the 0−3 V (vs. Li/Li^+) potential window at a scan rate of 0.2 mV s^{-1}. Upon the first discharge process, four cathodic peaks were detected. The peak at 0.67 V is ascribed to the formation of a solid electrolyte interphase (SEI) layer, since it is absence in the subsequent cycle.[33] The peaks at 0.27 and 0.13 V represent the stepwise electrochemical reactions of Ge with Li to form Li_xGe alloy, which is in consistent with the previous reports.[18,34] As for the 0.02 V peak, it comes from the insertion of Li^+ into graphene layers and the corresponding oxidation peak could be discerned at 0.12 V.[30] Besides the 0.12 V peak, a sharp peak at 0.58 V was also recorded in charge process, which is attributed to the oxidation of Li_xGe to Ge. Compared to the first cycle, the following curves have different shapes and the Li/Ge alloying peaks are located at 0.5 V, 0.36 V, 0.11 V. After the first cycle, the cycling curves largely overlap with each other, suggesting the high reversibility of the electrode reaction.

Galvanostatic discharge/charge tests were carried out to evaluate cycling performance of the Ge@graphene/VAGN electrodes. All the specific capacities were calculated based on the total mass of the electrode materials. Figure 3b shows voltage profiles of the 55 wt % sample at a current density of 260 mA g^{-1} within the potential range of 0.01−1.5 V. The initial discharge and charge capacities are 1840 and 860 mAh g^{-1}, respectively. The first discharge capacity is much higher than the theoretical value (1060 mAh g^{-1}, calculated by the equation: $C_{theoretical} = C_{Ge} \times wt_{Ge}\% + C_{VAGN} \times wt_{VAGN}\%$), leading to a relatively low initial Coulombic efficiency (ICE). Capacity loss in the first cycle and the low ICE should be ascribed to the formation of solid electrolyte interphase (SEI) films. During the initial discharge process, SEI films formed by side reaction between the active materials and the electrolyte, which trapped Li^+ inside the anode and caused irreversible capacity. Additionally, VAGN would contribute more SEI films due to its large surface area.[17,35,36] From the second cycle, Ge@graphene/VAGN electrode exhibited high stability performance (Figure 3c) and after a rapid increase in the several initial cycles, Coulombic efficiency of the electrode stabilized at ~97% for up to 90 cylces. The electrode delivered a capacity of 1014 mAh g^{-1} at the 90th cycle, indicating an excellent capacity retention of 97% compared with the second (1044 mAh g^{-1}).

For comparison, bare VAGN and Ge/VAGN were also tested. As shown in Figure 3c, bare VAGN exhibited stable cycling performance and delivered a capacity of 384 mAh g^{-1} after 90 cycles. Ge/VAGN electrode could show steady capacity of 890 mAh g^{-1} for more than 20 cycles but then the values gradually decreased. The capacity retention is 81% after 90 cycles. This comparison result suggests that graphene coatings play an important role in the cycling stability. Carbon coatings have been studied as buffer matrix to mitigate volume changes and most of the reported coatings possess thickness of 2−3 nm.[17,19] However, thanks to the excellent mechanical properties of graphene, it can well accommodate the expansion strain with 2−3 layers. Same results were also reported on few layer graphene coated Ge nanowires, indicating graphene is an ideal surface-protecting material.[37]

Rate performance of the Ge@graphene/VAGN electrode is shown in Figure 3d and the corresponding voltage profiles are shown in Supporting Information Figure S5. Current density was gradually increased from 0.22 A g^{-1} to 0.44, 0.88, 1.8, 3.6, 7.4, and 13 A g^{-1}, and stable rate capacities were recorded. Notably, the electrode could still deliver a capacity of 420 mAh g^{-1} at a high current density of 13 A g^{-1}, which is higher than that of commercial graphite. Finally, when current density returned to 220 mA g^{-1}, the capacity could recover to 997 mAh g^{-1}, suggesting a capacity retention of 94% to the initial value.

Figure 4 shows cycling performances of the 45% and 70 wt % samples under the same test condition. The former exhibits

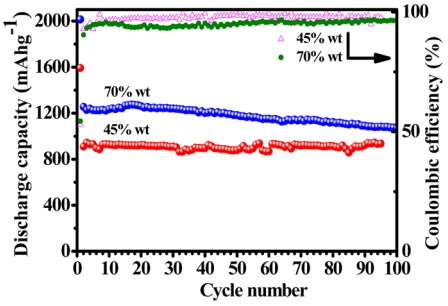

Figure 4. Cycling performance of the 45% and 70 wt % Ge content sample.

excellent cyclability, with nearly no capacity loss in 95 cycles. Though delivering higher capacity, the 70 wt % sample exhibited poor cycling stability. Its capacity stabilizes for 20 cycles and then begins to decrease. After 95 cycles, the capacity retention for 45% and 70 wt % sample is 100%, 84%, respectively.

To investigate the electrode changes upon cycling test, one cell at fully delthiated state was disassembled and observed by SEM and TEM. As Figure 5a shows, the nanosheets still keep vertical to the substrate and no graphene stacking is found. The dispersed nature of Ge NPs on VAGN could be seen in Figure 5b and c, indicating no particle aggregations occurred upon the lithiatin/delithiation process. More than 40 particles were measured to investigate their diameters after cycling. The statistical results are shown in Supporting Information Figure S6 and Table S4. According to the measurement, the average diameter of the postcycling NPs is 51 nm.

In the HRTEM image (Figure 5d), two changes could be seen. First, single crystalline Ge nanoparticle changed into polycrystalline structure. Inset is the two-dimensional fast Fourier transform (FFT) of the particle, a polycrystalline ring pattern could be clearly observed. Second, the graphene coating layer evolved into amorphous nature but still closely wraps the particle. Therefore, it can be envisaged that the coating layer expanded/shrank with particle expansion/contraction upon the cycling and successfully accommodated the particle volume change.

As a comparison, postcycling image of 70 wt % sample was also observed (Supporting Information Figure S7). It was found some particles were detached from the graphene sheets and aggregated together. That indicates upon cycling process, the mechanical strain resulted by volume changes exceeded the binding force between particle and flake. Since larger particles suffer more mechanical strain compared to smaller ones, they are easily detached. As we discussed in the introduction part, the aggregated particle will prolong the charge carrier path, even lead to insulation between the particle and current collector, finally cause capacity fading. That should be the reason why 70 wt % sample delivered poor capacity retention.

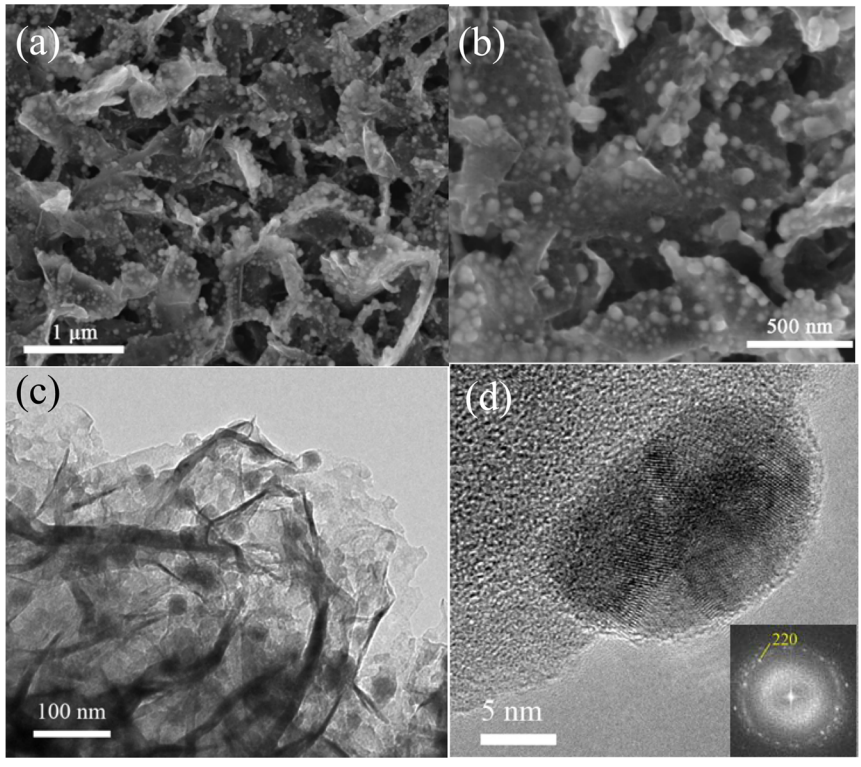

Figure 5. Postcycling morphologies of the Ge@graphene/VAGN electrode. (a) Low-magnification SEM image; (b) high-magnification SEM image; (c) low-magnification TEM image; (d) HRTEM of a particle, inset is the fast Fourier transform.

CONCLUSIONS

In summary, we have prepared a unique hybrid nanostructure, Ge@graphene/VAGN, to improve the cycling performance of Ge based anodes. Due to morphology nature of the sample, such as small particle size, monodispersion and graphene coatings, particle agglomeration and pulverization were successfully eliminated. Upon the discharge/charge process, the Ge@graphene/VAGN exhibits remarkable structure stability, which leads to the excellent cycling stability of the anodes. Therefore, our results display a promising approach to improve cyclability of the Li-alloying electrode materials.

ASSOCIATED CONTENT

Supporting Information

The detailed reaction conditions for three Ge-load samples (Table S1), the average mass of electrode materials (Table S2), cross-section SEM image of VAGN (Figure S1), energy dispersive X-ray spectroscopy (EDS) of the GeO_2/VAGN (Figure S2), SEM image of 45% and 70 wt % sample (Figure S3), diameter measurement of Ge NPs before and post cycling (Figure S4, S6, Table S3, S4), voltage profiles for rate test (Figure S5), and postcycling SEM image of 70 wt % sample (Figure S7). This material is available free of charge via the Internet at http://pubs.acs.org/.

AUTHOR INFORMATION

Corresponding Author

*E-mail: wchengx@mail.sysu.edu.cn.

Notes

The authors declare no competing financial interest.

ACKNOWLEDGMENTS

This work was financially supported by the National Nature Science Foundation of China (51125008, 11274392).

REFERENCES

(1) Wu, X. L.; Guo, Y. G.; Wan, L. J. Rational Design of Anode Materials Based on Group IVA Elements (Si, Ge, and Sn) for Lithium-Ion Batteries. *Chem.—Asian J.* **2013**, *8*, 1948−1958.

(2) Vaughn, D. D., II; Schaak, R. E. Synthesis, Properties, and Applications of Colloidal Germanium and Germanium-Based Nanomaterials. *Chem. Soc. Rev.* **2013**, *42*, 2861−2879.

(3) Park, C. M.; Kim, J. H.; Kim, H.; Sohn, H. J. Li-Alloy Based Anode Materials for Li Secondary Batteries. *Chem. Soc. Rev.* **2010**, *39*, 3115−3141.

(4) Graetz, J.; Ahn, C. C.; Yazami, R.; Fultz, B. Nanocrystalline and Thin Film Germanium Electrodes with High Lithium Capacity and High Rate Capabilities. *J. Electrochem. Soc.* **2004**, *151*, A698−A702.

(5) Wang, Z. Y.; Wang, Z. C.; Liu, W. T.; Xiao, W.; Lou, X. W. Amorphous $CoSnO_3$@C Nanoboxes with Superior Lithium Storage Capability. *Energy Environ. Sci.* **2013**, *6*, 87−91.

(6) Yoon, S.; Park, C. M.; Sohn, H. J. Electrochemical Characterizations of Germanium and Carbon-Coated Germanium Composite Anode for Lithium-Ion Batteries. *Electrochem. Solid-State Lett.* **2008**, *11*, A42−A45.

(7) Yang, L. C.; Gao, Q. S.; Li, L.; Tang, Y.; Wu, Y. P. Mesoporous Germanium as Anode Material of High Capacity and Good Cycling Prepared by a Mechanochemical Reaction. *Electrochem. Commun.* **2010**, *12*, 418−421.

(8) Park, M. H.; Kim, K.; Kim, J.; Cho, J. Flexible Dimensional Control of High-Capacity Li-Ion-Battery Anodes: From 0D Hollow to 3D Porous Germanium Nanoparticle Assemblies. *Adv. Mater.* **2010**, *22*, 415−418.

(9) Cui, G. L.; Gu, L.; Zhi, L. J.; Kaskhedikar, N.; van Aken, P. A.; Müllen, K.; Maier, J. A Germanium−Carbon Nanocomposite Material for Lithium Batteries. *Adv. Mater.* **2008**, *20*, 3079−3083.

(10) Jo, G.; Choi, I.; Ahn, H.; Park, M. J. Binder-Free Ge Nanoparticles−Carbon Hybrids for Anode Materials of Advanced Lithium Batteries with High Capacity and Rate Capability. *Chem. Commun.* **2012**, *48*, 3987−3989.

(11) Cheng, J. S.; Du, J. Facile Synthesis of Germanium−Graphene Nanocomposites and Their Application as Anode Materials for Llithium Ion Batteries. *CrystEngComm* **2012**, *14*, 397−400.

(12) DiLeo, R. A.; Frisco, S.; Ganter, M. J.; Rogers, R. E.; Raffaelle, R. P.; Landi, B. J. Hybrid Germanium Nanoparticle−Single-Wall Carbon Nanotube Free-Standing Anodes for Lithium Ion Batteries. *J. Phys. Chem. C* **2011**, *115*, 22609−22614.

(13) Ko, Y. D.; Kang, J. G.; Lee, G. H.; Park, J. G.; Park, K. S.; Jin, Y. H.; Kim, D. W. Sn-Induced Low-Temperature Growth of Ge Nanowire Electrodes with a Large Lithium Storage Capacity. *Nanoscale* **2011**, *3*, 3371−3375.

(14) Chan, C. K.; Zhang, X. F.; Cui, Y. High Capacity Li Ion Battery Anodes Using Ge Nanowires. *Nano Lett.* **2008**, *8*, 307−309.

(15) Park, M. H.; Cho, Y.; Kim, K.; Kim, J.; Liu, M.; Cho, J. Germanium Nanotubes Prepared by Using the Kirkendall Effect as Anodes for High-Rate Lithium Batteries. *Angew. Chem., Int. Ed.* **2011**, *50*, 9647−9650.

(16) Hwang, I. S.; Kim, J. C.; Seo, S. D.; Lee, S.; Lee, J. H.; Kim, D. W. A Binder-Free Ge-Nanoparticle Anode Assembled on Multiwalled Carbon Nanotube Networks for Li-Ion Batteries. *Chem. Commun.* **2012**, *48*, 7061−7063.

(17) Xue, D. J.; Xin, S.; Yan, Y.; Jiang, K. C.; Yin, Y. X.; Guo, Y. G.; Wan, L. J. Improving the Electrode Performance of Ge through Ge@C Core-Shell Nanoparticles and Graphene Networks. *J. Am. Chem. Soc.* **2012**, *134*, 2512−2515.

(18) Wang, Y.; Wang, G. X. Facile Synthesis of Ge@C Core-Shell Nanocomposites for High-Performance Lithium Storage in Lithium-Ion Batteries. *Chem.—Asian J.* **2013**, *8*, 3142−3146.

(19) Li, D.; Seng, K. H.; Shi, D. Q.; Chen, Z. X.; Liu, H. K.; Guo, Z. P. A Unique Sandwich-Structured C/Ge/Graphene Nanocomposite as an Anode Material for High Power Lithium Ion Batteries. *J. Mater. Chem. A* **2013**, *1*, 14115−14121.

(20) Zhou, M.; Cai, T. W.; Pu, F.; Chen, H.; Wang, Z.; Zhang, H. Y.; Guan, S. Y. Graphene/Carbon-Coated Si Nanoparticle Hybrids as High-Performance Anode Materials for Li-Ion Batteries. *ACS Appl.Mater. Interfaces* **2013**, *5*, 3449−3455.

(21) Sun, C.; Deng, Y. F.; Wan, L.; Qin, X. S.; Chen, G. H. Graphene Oxide-Immobilized NH_2-Terminated Silicon Nanoparticles by Cross-Linked Interactions for Highly Stable Silicon Negative Electrodes. *ACS Appl.Mater. Interfaces* **2014**, *6*, 11277−11285.

(22) Xiao, X. C.; Liu, P.; Wang, J. S.; Verbrugge, M. W.; Balogh, M. P. Vertically Aligned Graphene Electrode for Lithium Ion Battery with High Rate Capability. *Electrochem. Commun.* **2011**, *13*, 209−212.

(23) Li, N.; Song, H. W.; Cui, H.; Yang, G. W.; Wang, C. X. Self-Assembled Growth of Sn@CNTs on Vertically Aligned Graphene for Binder-Free High Li-Storage and Excellent Stability. *J. Mater. Chem. A* **2014**, *2*, 2526−2537.

(24) Jin, S. X.; Li, N.; Cui, H.; Wang, C. X. Growth of the Vertically Aligned Graphene@ Amorphous GeOx Sandwich Nanoflakes and Excellent Li Storage Properties. *Nano Energy* **2013**, *2*, 1128−1136.

(25) Malesevic, A.; Vitchev, R.; Schouteden, K.; Volodin, A.; Zhang, L.; Tendeloo, G. V.; Vanhulsel, A.; Haesendonck, C. V. Synthesis of Few-Layer Graphene via Microwave Plasma-Enhanced Chemical Vapor Deposition. *Nanotechnology* **2008**, *19*, 305604.

(26) Wang, J. J.; Zhu, M. Y.; Outlaw, R. A.; Zhao, X.; Manos, D. M.; Holloway, B. C.; Mammana, V. P. Free-Standing Subnanometer Graphite Sheets. *Appl. Phys. Lett.* **2004**, *85*, 1265−1267.

(27) Zheng, M. B.; Qiu, D. F.; Zhao, B.; Ma, L. Y.; Wang, X. R.; Lin, Z. X.; Pan, L. J.; Zheng, Y. D.; Shi, Y. Mesoporous Iron Oxide Directly Anchored on a Graphene Matrix for Lithium-Ion Battery Anodes with Enhanced Strain Accommodation. *RSC Adv.* **2013**, *3*, 699−703.

(28) Seng, K. H.; Park, M. H.; Guo, Z. P.; Liu, H. K.; Cho, J. Catalytic Role of Ge in Highly Reversible GeO_2/Ge/C Nanocomposite Anode Material for Lithium Batteries. *Nano Lett.* **2013**, *13*, 1230−1236.
(29) Jing, C. B.; Zhang, C. J.; Chu, J. H. Formation and Characterization of Nanoporous Structures on Surface of LPD-Derived GeO_2 Ceramic Film. *J. Porous. Mater.* **2012**, *20*, 359−365.
(30) Wang, C. D.; Chui, Y. S.; Li, Y.; Chen, X. F.; Zhang, W. J. Binder-Free Ge-Three Dimensional Graphene Electrodes for High-Rate Capacity Li-Ion Batteries. *Appl. Phys. Lett.* **2013**, *103*, 253903.
(31) Li, N.; Song, H. W.; Cui, H.; Wang, C. X. SnO_2 Nanoparticles Anchored on Vertically Aligned Graphene with a High Rate, High Capacity, and Long Life for Lithium Storage. *Electrochim. Acta* **2014**, *130*, 670−678.
(32) Yao, F.; Gunes, F.; Ta, H. Q.; Lee, S. M.; Chae, S. J.; Sheem, K. Y.; Cojocaru, C. S.; Xie, S. S.; Lee, Y. H. Diffusion Mechanism of Lithium Ion through Basal Plane of Layered Graphene. *J. Am. Chem. Soc.* **2012**, *134*, 8646−8654.
(33) Liu, X.; Zhao, J. P.; Hao, J.; Su, B. L.; Li, Y. 3D Ordered Macroporous Germanium Fabricated by Electrodeposition from an Ionic Liquid and Its Lithium Storage Properties. *J. Mater. Chem. A* **2013**, *1*, 15076−15081.
(34) Laforge, B.; Levan-Jodin, L.; Salot, R.; Billard, A. Study of Germanium as Electrode in Thin-Film Battery. *J. Electrochem. Soc.* **2008**, *155*, A181−A188.
(35) Yuan, F. W.; Tuan, H. Y. Scalable Solution-Grown High-Germanium-Nanoparticle-Loading Graphene Nanocomposites as High-Performance Lithium-Ion Battery Electrodes: An Example of a Graphene-Based Platform toward Practical Full-Cell Applications. *Chem. Mater.* **2014**, *26*, 2172−2179.
(36) Zhong, C.; Wang, J. Z.; Gao, X. W.; Wexler, D.; Liu, H. K. In Situ One-Step Synthesis of a 3D Nanostructured Germanium−Graphene Composite and Its Application in Lithium-Ion Batteries. *J. Mater. Chem. A* **2013**, *1*, 10798−10804.
(37) Kim, H.; Son, Y.; Park, C.; Cho, J.; Choi, H. C. Catalyst-Free Direct Growth of a Single to a Few Layers of Graphene on a Germanium Nanowire for the Anode Material of a Lithium Battery. *Angew. Chem., Int. Ed.* **2013**, *52*, 5997−6001.